© 2014. Published by The Company of Biologists Ltd | Journal of Cell Science (2014) 127, 4009–4023 doi:10.1242/jcs.150987

RESEARCH ARTICLE

Rho/ROCK pathway inhibition by the CDK inhibitor p27^{kip1} participates in the onset of macrophage 3D-mesenchymal migration

Philippe Gui[1,2], Arnaud Labrousse[1,2], Emeline Van Goethem[1,2], Arnaud Besson[3], Isabelle Maridonneau-Parini[1,2,*] and Véronique Le Cabec[1,2]

ABSTRACT

Infiltration of macrophages into tissue can promote tumour development. Depending on the extracellular matrix architecture, macrophages can adopt two migration modes: amoeboid migration – common to all leukocytes, and mesenchymal migration – restricted to macrophages and certain tumour cells. Here, we investigate the initiating mechanisms involved in macrophage mesenchymal migration. We show that a single macrophage is able to use both migration modes. Macrophage mesenchymal migration is correlated with decreased activity of Rho/Rho-associated protein kinase (ROCK) and is potentiated when ROCK is inhibited, suggesting that amoeboid inhibition participates in mechanisms that initiate mesenchymal migration. We identify the cyclin-dependent kinase (CDK) inhibitor p27^{kip1} (also known as CDKN1B) as a new effector of macrophage 3D-migration. By using p27^{kip1} mutant mice and small interfering RNA targeting p27^{kip1}, we show that p27^{kip1} promotes mesenchymal migration and hinders amoeboid migration upstream of the Rho/ROCK pathway, a process associated with a relocation of the protein from the nucleus to the cytoplasm. Finally, we observe that cytoplasmic p27^{kip1} is required for *in vivo* infiltration of macrophages within induced tumours in mice. This study provides the first evidence that silencing of amoeboid migration through inhibition of the Rho/ROCK pathway by p27^{kip1} participates in the onset of macrophage mesenchymal migration.

KEY WORDS: Macrophage, 3D-migration, Amoeboid, Mesenchymal, Rho/ROCK pathway, p27^{kip1}, CDKN1B

INTRODUCTION

Tissue infiltration by macrophages plays a central role in initiation and progression of immune and inflammatory responses, clearance of microorganisms and tissue repair. However, macrophages also promote the development of pathologies, such as chronic inflammatory diseases (Elkington and Friedland, 2006; Maruotti et al., 2007), atherosclerosis (Weber et al., 2008) and cancer (Porta et al., 2011), by causing tissue lesions (Luster et al., 2005; Pollard, 2009) or by enhancing tumour growth and formation of metastases (Pollard, 2009; Porta et al., 2011). Therefore, specific control of macrophage tissue infiltration has been proposed as a new anti-inflammatory and anti-cancer strategy (Mackay, 2008; Qualls and Murray, 2010; Ruhrberg and De Palma, 2010).

When macrophages migrate in order to reach tissue sites, they are confronted with many different environments that can either be two-dimensional (2D) on the vascular endothelium, the lumen of peritoneum and the pleura; or three-dimensional (3D) inside tissues comprising cellular components and extracellular matrix (ECM). The interstitial ECM is primarily composed of collagen I fibres that are crosslinked into a stable mesh (Even-Ram and Yamada, 2005; Schindler et al., 2006), ranging from loose fibrillar regions to densely compacted connective tissue with submicron spacing (Friedl and Weigelin, 2008; Kalluri, 2003; Schindler et al., 2006). In addition, the biophysical properties of tissues can vary during the progression of a disease; for example remodelling of the ECM during tumour development leads to tissue stiffening (DuFort et al., 2011).

It has been established that 2D and 3D cell migration involve distinct mechanisms (Doyle et al., 2009). By using several types of ECM, we have recently shown that, depending on the matrix architecture, human monocyte-derived macrophages (hMDMs) are capable of employing the two modes of 3D-migration originally described for tumour cells (Van Goethem et al., 2010). Amoeboid migration commonly refers to rounded or ellipsoid cells that slide through matrix pores, and show little to no adhesion to the matrix (Friedl and Wolf, 2003; Sahai and Marshall, 2003); it is triggered in macrophages that migrate through loose matrices, such as fibrillar collagen (Van Goethem et al., 2010). In contrast, mesenchymal migration is characterised by an elongated cell shape with membrane protrusions and proteolytic matrix degradation (Friedl and Wolf, 2003; Sahai and Marshall, 2003), and it is only triggered in macrophages migrating through dense matrices such as Matrigel, gelled collagen or native collagen (Van Goethem et al., 2010; Wiesner et al., 2014). Whereas amoeboid migration has been described for all leukocytes, macrophages appear to be the only leukocytes that are able to utilise mesenchymal migration (Cougoule et al., 2012). Therefore, this migration mode represents a promising pharmacological target for specific control of macrophage tissue infiltration and deserves broader characterisation.

Like tumour cell amoeboid migration, macrophage amoeboid migration is dependent on Rho-associated protein kinase (ROCK) activity and independent of protease-mediated ECM degradation (Van Goethem et al., 2010). In contrast, macrophage mesenchymal migration is inhibited by protease inhibitors but not

[1]Centre National de la Recherche Scientifique (CNRS), IPBS (Institut de Pharmacologie et de Biologie Structurale), 205 route de Narbonne, BP64182, F-31077 Toulouse, France. [2]Université de Toulouse, UPS, IPBS, F-31077 Toulouse, France. [3]INSERM UMR1037-Cancer Research Center of Toulouse, Université de Toulouse, CNRS ERL5294, Toulouse, France.

*Author for correspondence (isabelle.maridonneau-parini@ipbs.fr)

Received 3 February 2014; Accepted 4 July 2014

Journal of Cell Science

Journal of Cell Science (2014) 127, 4009–4023 doi:10.1242/jcs.150987

by ROCK inhibitors (Van Goethem et al., 2010). In contrast to tumour cell mesenchymal migration, which mainly depends on matrix metalloprotease (MMP) activity, macrophage mesenchymal migration can be mediated by other protease families, including lysosomal cysteine cathepsins (Jevnikar et al., 2012; Van Goethem et al., 2010), in addition to MMPs such as MT1-MMP (Guiet et al., 2011; Wiesner et al., 2013). Macrophage mesenchymal migration, but not amoeboid migration, is also dependent on Hck (Cougoule et al., 2010), Filamin-A (Guiet et al., 2012) and 3D-podosomes (Van Goethem et al., 2011).

To further characterise macrophage 3D-mesenchymal migration, we examined the mechanisms that participate in specifically triggering this migration mode within dense matrices. It has been shown that tumour cells can spontaneously employ mesenchymal or amoeboid migration within porous or dense matrices depending on the cell line (Carragher et al., 2006; Sahai and Marshall, 2003). In addition, typical mesenchymal tumour cell lines, such as HT1080 cells, BE colon carcinoma cells or WM266.4 melanoma cells, can overcome mesenchymal migration inhibitors by switching to amoeboid migration. In contrast, we have shown in a previous study that macrophages adapt their migration mode to the matrix architecture and that, in a given matrix, essentially one migration mode is observed (Van Goethem et al., 2010). In addition, pharmacological inhibition of macrophage mesenchymal migration did not induce a switch to amoeboid migration in dense matrices (Van Goethem et al., 2010) as opposed to tumour cells (Carragher et al., 2006; Friedl and Wolf, 2003; Sahai and Marshall, 2003), suggesting that amoeboid migration is switched off. Finally, in a given matrix, only part of the initial macrophage population was able to migrate; after 72 h, the percentage of macrophage migration rarely exceeded 40%. Altogether, these observations lead us to propose the following: either, 1) triggering of macrophage mesenchymal migration in dense matrices is restricted to one particular macrophage subpopulation or, 2) all migrating macrophages are able to use both migration modes but only activate mesenchymal migration upon contact with dense matrices while silencing amoeboid migration.

In this present study, we investigate these two hypotheses and show that a single macrophage is able to employ both mesenchymal and amoeboid migration. In addition, macrophage mesenchymal migration is correlated with a decreased Rho/ROCK activity and is enhanced by ROCK inhibition, which suggests that amoeboid migration inhibition participates in the onset of macrophage mesenchymal migration. By searching for possible molecular effectors of this process, we took interest in the cyclin-dependent kinase (CDK) inhibitor $p27^{kip1}$ (also known as CDKN1B), because it has been previously shown to be involved in 2D cell migration through inhibition of RhoA (Besson et al., 2004b). Accordingly, we identify $p27^{kip1}$ as a new effector of macrophage 3D-migration *in vitro* and *in vivo* that acts upstream of the Rho/ROCK pathway in order to potentiate mesenchymal migration, probably by inhibiting amoeboid migration.

RESULTS

A single macrophage can employ both amoeboid and mesenchymal migration

We first examined whether a single macrophage can employ both migration modes or whether triggering of mesenchymal migration in dense matrices is restricted to one particular subpopulation of macrophages that cannot employ amoeboid migration. We, therefore, designed a composite matrix that comprised gelled collagen (pore size <1 μm) polymerised on top of fibrillar collagen (pore size >2 μm) (Fig. 1). We have previously shown that macrophages utilise mesenchymal migration in gelled collagen, like in Matrigel, and amoeboid migration in fibrillar collagen (Van Goethem et al., 2010). hMDMs started to infiltrate gelled collagen 24 h after being seeded on top of the composite matrix, by employing mesenchymal migration – as attested by elongated and protrusive cell morphology that was observed by using time-lapse video-microscopy (Fig. 1, white arrow). Once they reached the interface between the two matrices, hMDMs proceeded to migrate into the fibrillar collagen layer by employing amoeboid migration, as evidenced by their round cell shape (Fig. 1, black arrow). The reverse was observed when hMDMs were seeded on a composite matrix made of fibrillar collagen polymerised on the top of Matrigel (data not shown). These results show that a single hMDM is able to use both modes of migration by adapting to the matrix architecture, and that mesenchymal and amoeboid migration are not restricted to distinct macrophage subpopulations.

Macrophage mesenchymal migration is potentiated by the ROCK inhibitor Y27632 and correlates with decreased Rho/ROCK activity

Since a single macrophage is capable of employing both migration modes but only uses mesenchymal migration in matrices where amoeboid migration is not spontaneously activated, we next hypothesised that silencing of amoeboid migration triggers mesenchymal migration. Therefore, we investigated whether inhibition of a key effector of amoeboid migration facilitates macrophage mesenchymal migration through dense matrices.

Given that amoeboid migration has been defined as a Rho/ROCK-dependent migration mode – as opposed to mesenchymal migration, which is Rho/ROCK-independent – a dose-response assay with the ROCK inhibitor Y27632 on macrophage 3D-migration was performed. The percentage of macrophages migrating inside the matrix was measured at different time points to evaluate the capacity of cells to initiate ECM infiltration. As shown on Fig. 2A, Y27632 inhibited amoeboid migration very efficiently in fibrillar collagen as expected since macrophages cannot employ mesenchymal migration upon inhibition of amoeboid migration in fibrillar collagen (Van Goethem et al., 2010). This is in sharp contrast with some tumor cell lines that can, indeed, employ mesenchymal migration by default in porous matrices (Carragher et al., 2006; Sahai and Marshall, 2003). However, in Matrigel, Y27632 significantly increased the percentage of migrating cells that used mesenchymal migration. A comparable increase was obtained with macrophages that migrated through gelled collagen – another dense matrix that triggers mesenchymal migration ($158\pm16\%$ and $256\pm101\%$ of control at 20 μM and 40 μM Y27632, respectively; measured after 48 h of migration, mean± s.d., macrophages of three independent donors). This shows that inhibition of the Rho/ROCK pathway increases the percentage of macrophages that infiltrate dense matrices by using mesenchymal migration.

Distance of macrophage migration inside matrices was then used as an indicator of migration efficiency (Fig. 2B). Y27632 strongly decreased the migration distance in fibrillar collagen. In Matrigel, Y27632 did not increase the migration distance concurrently with the percentage of migration, but decreased it

Journal of Cell Science (2014) 127, 4009–4023 doi:10.1242/jcs.150987

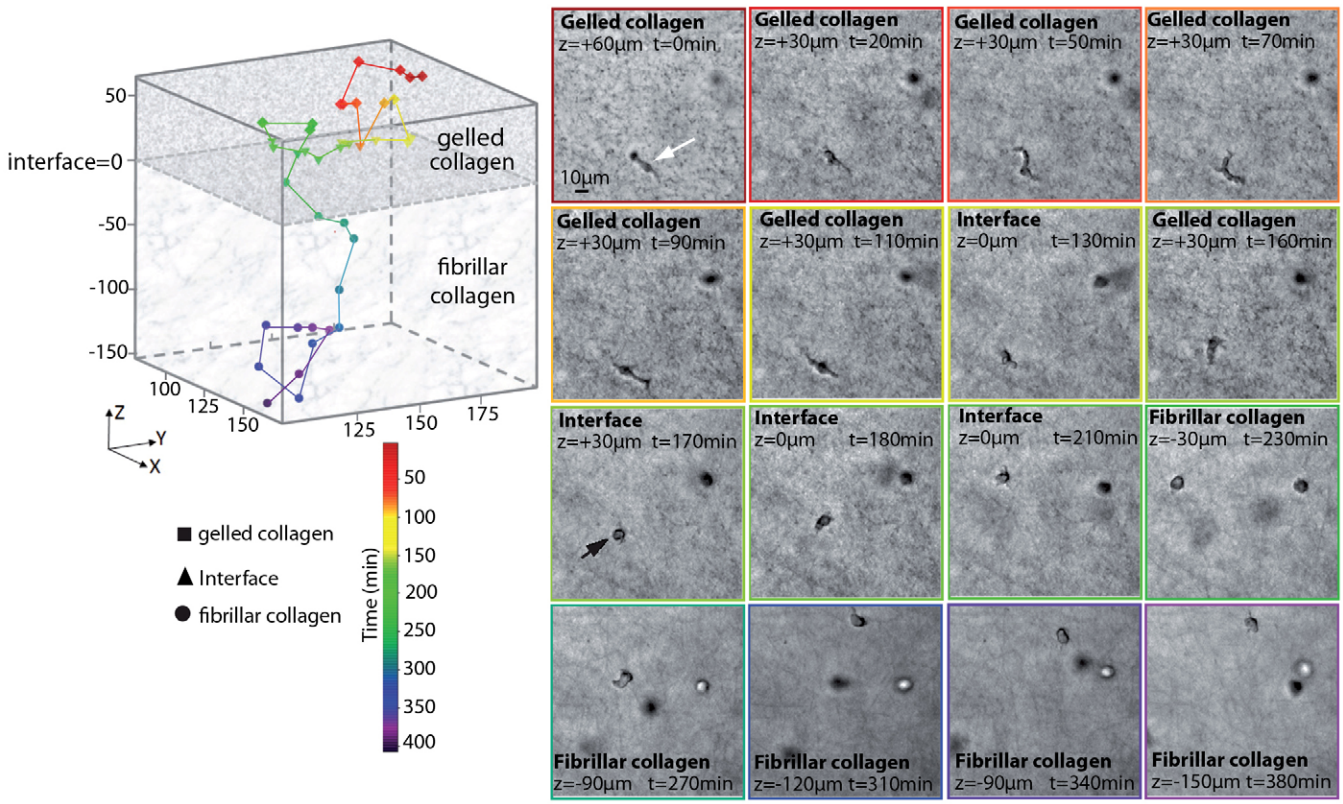

Fig. 1. A single hMDM can undergo both mesenchymal and amoeboid migration. hMDMs were loaded on a thick layer of gelled collagen polymerised on top of fibrillar collagen I. Cell migration was scored on day 3, and photographs of a single representative hMDM (white arrow, first picture) were collected every 10 min for 380 min using an inverted video-microscope, from the gelled collagen layer (z=+60 µm to 0 µm) to the fibrillar collagen layer (z=0 µm to −150 µm). The x,y,z path followed by the cell in the matrices is shown in the 3D reconstitution diagram. A single hMDM was tracked and each point corresponds to its position at a given time. Squares correspond to the hMDM migrating in gelled collagen, triangles to the hMDM present at the interface between the two matrices and circles to the hMDM migrating through fibrillar collagen. The colour spectre range indicates the time scale. During the first 24 h hMDMs stayed on top of the gelled collagen and then migrated through the dense matrix using mesenchymal migration. At the interface, the hMDMs tended to return to the gelled collagen layer several times before shifting to amoeboid migration (black arrow) into the fibrillar collagen layer.

slightly. This indicates that inhibition of the Rho/ROCK pathway activates dense matrices infiltration by mesenchymal migration but not efficiency of this migration process per se.

Next, we investigated the effect of Y27632 on macrophage morphology in Matrigel (Fig. 2C). Control macrophages mainly show a round morphology when on top of Matrigel and an elongated morphology when inside, with 25% of migrating hMDMs remaining round; a morphology characteristic of amoeboid migration (Fig. 2C, arrows) (Van Goethem et al., 2010). In the presence of Y27632, macrophages on top of the matrix acquired a protrusive phenotype (Fig. 2C, images on the left). It also significantly reduced the percentage of round hMDMs inside Matrigel (Fig. 2C, graph). This suggests that, in addition to its potentiating effect on the number of hMDMs that employ mesenchymal migration, ROCK inhibition decreases the number of hMDMs that utilise Rho/ROCK-dependent amoeboid migration in dense matrices.

We next investigated Rho activity during macrophage 3D-mesenchymal migration and compared it to Rho activity during amoeboid migration, by performing western blot analysis of the phosphorylation states of two reliable markers of this pathway, cofilin and Ezrin–radixin–moesin (ERM) (Fuster et al., 2011; Takai et al., 2001). Migrating macrophages were lysed by boiling Laemmli buffer directly in matrices. Consequently, high amounts of proteins had to be loaded on gels to detect macrophage proteins, explaining the poorly resolved immunoblots that are shown. The ratios of phospho-cofilin to cofilin and of phospho-ERM to ERM were reduced in macrophages migrating through gelled collagen and Matrigel compared to those migrating through fibrillar collagen (Fig. 2D,E). These results indicate that there is a significant reduction of the Rho/ROCK pathway activity during macrophage mesenchymal migration compared to amoeboid migration, which further suggests that inhibition of this signalling pathway is one of the mechanisms that triggers mesenchymal migration.

$p27^{kip1}$ is a regulator of macrophage 3D-migration that triggers mesenchymal migration in dense matrices and reduces amoeboid migration efficiency in fibrillar collagen

It has previously been shown that the CDK inhibitor $p27^{kip1}$ regulates tumour cell migration (Berton et al., 2009) through inhibition of the Rho/ROCK pathway in 2D environments (Besson et al., 2004b). $p27^{kip1}$ interacts with RhoA, thereby blocking its activation by Rho guanine nucleotide-exchange factors. We, therefore, investigated whether $p27^{kip1}$ is an effector of amoeboid migration inhibition during macrophage mesenchymal migration.

We first analysed $p27^{kip1}$ expression levels in macrophages plated on 2D coverslips, or employing either amoeboid migration or mesenchymal migration in 3D matrices. Western blot analyses showed that $p27^{kip1}$ was upregulated in hMDMs migrating

Journal of Cell Science (2014) 127, 4009–4023 doi:10.1242/jcs.150987

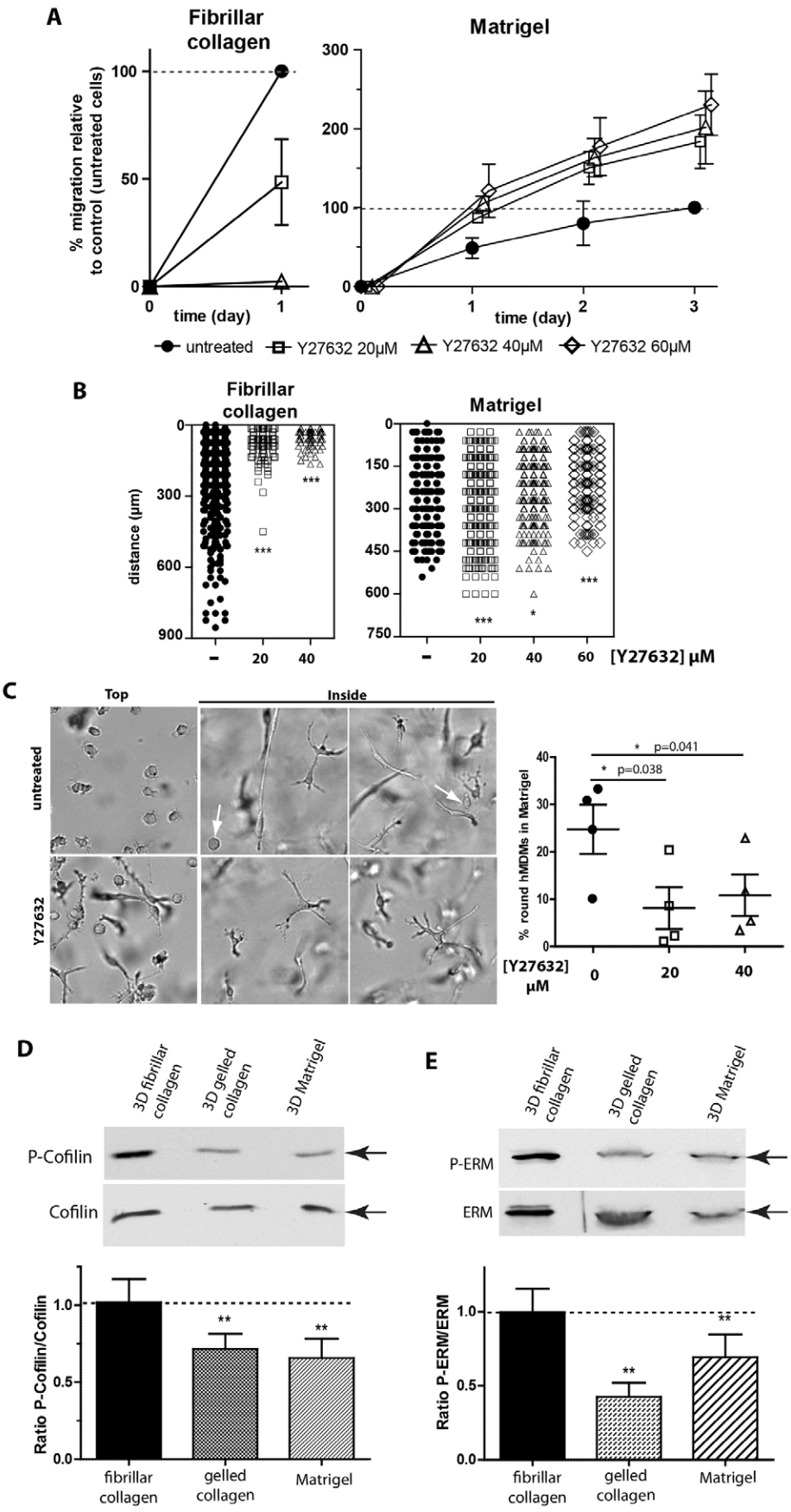

Fig. 2. Macrophage mesenchymal migration is potentiated following treatment with Y27632 and is correlated with decreased Rho/ROCK activity. (A,B) Dose-dependent effect of the ROCK inhibitor Y27632 on the percentage of hMDM migration (A) and the distance of migration (B) through fibrillar collagen or Matrigel. Migration experiments were conducted in the presence of indicated concentrations of Y27632. In A, results were normalised to the percentage of migration obtained with untreated macrophages at 24 h for fibrillar collagen and 72 h for Matrigel. Mean ± s.d. of four independent donors are shown. For the *z*-distribution (B), each point represents the *z*-position (μm) of one hMDM within the matrix (0 representing the surface of the matrix). Statistics: paired Student's *t*-test, two-tailed, 95% confidence interval. $^{**}P=0.009$ and $^{*}P=0.047$ (A); $^{*}P=0.026$ and 0.020 (B) in gelled collagen and Matrigel, respectively). (C) The morphology of macrophages migrating through Matrigel in the presence or absence of Y27632 was assessed. The effect of the ROCK inhibitor on cell morphology on the top (left images) or inside Matrigel (middle and right images) is shown. The percentage of macrophages showing a round morphology inside the matrix (arrows) was quantified (graph). (D,E) Western blot analysis of cofilin, phosphorylated cofilin (C), ERM and phosphorylated ERM (D) in hMDMs from eight (D) or ten (C) independent donors, within 3D fibrillar collagen, 3D gelled collagen I and Matrigel following 3D-migration. Ratio of phospho-protein to total protein signal was calculated and normalised to the ratios scored in fibrillar collagen. Mean ± s.e.m. are shown. Representative immunoblots are shown. Statistics: paired Student's *t*-test, two-tailed, 95% confidence interval. $^{**}P=0.0015$ for gelled collagen and $P=0.0042$ for Matrigel (C); $^{**}P=0.0012$ for gelled collagen and $P=0.009$ for Matrigel (D).

Journal of Cell Science

Journal of Cell Science (2014) 127, 4009–4023 doi:10.1242/jcs.150987

through 3D gelled collagen or Matrigel (mesenchymal migration) compared to 3D fibrillar collagen (amoeboid migration) or 2D coverslips (Fig. 3A). This suggests that $p27^{kip1}$ is specifically required for macrophage mesenchymal migration. It is worth noticing that western blot analyses were performed by using the entire macrophage population, of which ~40% were able to infiltrate the matrix after 72 h, suggesting that the measured $p27^{kip1}$ upregulation is an underestimation.

To investigate the role of $p27^{kip1}$ in macrophage 3D-migration, we next compared the migration capabilities of bone-marrow-derived macrophages (BMDMs) isolated from wild-type ($p27^{kip1+/+}$) and $p27^{kip1}$-deficient ($p27^{kip1-/-}$) mice (Fero et al., 1996). These experiments were performed in either fibrillar collagen or Matrigel, in which mouse BMDMs – similarly to hMDMs – have been shown to use amoeboid or mesenchymal migration, respectively (Guiet et al., 2012). The percentage of cells migrating through Matrigel was significantly reduced in $p27^{kip1-/-}$ BMDMs compared to $p27^{kip1+/+}$ BMDMs (Fig. 3B). We then measured the migration distance of $p27^{kip1-/-}$ BMDMs that were still able to migrate through Matrigel and observed that it was unchanged compared to wild-type cells (Fig. 3C). This indicates that $p27^{kip1}$ – similar to pharmacological ROCK inhibition – increases the percentage of macrophages that are able to trigger mesenchymal migration but not the efficiency of the migration process by itself. In contrast, the percentage of $p27^{kip1-/-}$ BMDMs using amoeboid migration in fibrillar collagen was not significantly different compared to $p27^{kip1+/+}$ BMDMs (Fig. 3D). However, the distance of migration was significantly increased, with the maximal distance being 500 and 800 µm, and the deeper 20th percentile being 255 and 300 µm in $p27^{kip1+/+}$ and $p27^{kip1-/-}$ BMDMs, respectively (Fig. 3E). This suggests that $p27^{kip1}$ does not control the ability of macrophages to employ amoeboid migration in fibrillar collagen but, rather, decreases the migration efficiency of macrophages once inside the matrix.

Comparable results were obtained with hMDMs in which $p27^{kip1}$ expression was reduced by using a specific small interfering RNA (siRNA) targeting $p27^{kip1}$ (Fig. 3F,G). In the timeframe (48–72 h) during which the expression of $p27^{kip1}$ was reduced to 0.6-fold of control levels (Fig. 3F), the percentage of macrophages migrating in Matrigel was found to be decreased compared to cells transfected with a scrambled siRNA as a control (Fig. 3G). Similar results were observed in gelled collagen (Fig. 3G). Together, these results show that $p27^{kip1}$ is part of the macrophage 3D-migration machinery that promotes mesenchymal migration and reduces amoeboid migration efficiency.

$p27^{kip1}$ deficiency is counterbalanced by pharmacological ROCK inhibition and induces a mesenchymal-to-amoeboid migration switch in dense matrices

Given that $p27^{kip1}$ is described as an inhibitor of the Rho/ROCK signalling pathway (Besson et al., 2004b), we hypothesised that its positive effect on macrophage mesenchymal migration through dense matrices occurs through RhoA inhibition and, therefore, amoeboid migration silencing. As a consequence, $p27^{kip1}$ deficiency should have two main effects on macrophage migration: 1) it should promote macrophage amoeboid migration in dense matrices, such as Matrigel and, 2) its inhibitory effect on mesenchymal migration should be reversed by restoring the inhibition of the Rho/ROCK pathway with a ROCK inhibitor.

To explore these hypotheses, we analysed the percentage of migration of $p27^{kip1-/-}$ BMDMs and $p27^{kip1+/+}$ BMDMs in Matrigel and fibrillar collagen in the presence or absence of Y27632. In these experiments, the proportion of round BMDMs migrating through Matrigel was also scored and used as an indicator of amoeboid migration in this dense matrix. In fibrillar collagen, BMDMs from $p27^{kip1+/+}$ and $p27^{kip1-/-}$ mice both adopted the typical round amoeboid-like shape (Fig. 4A, top). In Matrigel, both cell genotypes mainly exhibited an elongated spindle shape, with F-actin clusters being observed at the tips of membrane protrusions, as previously described in human macrophages employing mesenchymal migration (Fig. 4A, bottom, arrowheads). However, we observed a significant increase in the percentage of round BMDMs in $p27^{kip1-/-}$ compared to $p27^{kip1+/+}$ BMDMs in Matrigel (Fig. 4B). Similar results were obtained with hMDMs upon $p27^{kip1}$ silencing (Fig. 4C). This suggests that amoeboid migration is, indeed, activated in macrophages that are still able to migrate through Matrigel in the absence of $p27^{kip1}$.

As expected, Y27632 (10 µM) efficiently inhibited amoeboid migration (percentage of migration and migration distance) of both $p27^{kip1+/+}$ and $p27^{kip1-/-}$ BMDMs in fibrillar collagen (Fig. 4D). In Matrigel, Y27632 had no significant effect on $p27^{kip1+/+}$ BMDM migration (percentage of migration and percentage of round cells) as predicted (Fig. 4E, left). In contrast, the reduced migration ability of $p27^{kip1-/-}$ BMDMs and the increased number of round $p27^{kip1-/-}$ BMDMs were completely restored to control levels by Y27632 (Fig. 4E, right) showing that pharmacological ROCK inhibition is able to counterbalance $p27^{kip1}$ deficiency.

Altogether, these results show that $p27^{kip1}$ deficiency, in addition to its inhibitory effect on macrophage mesenchymal migration through dense matrices, prompts macrophages to adopt amoeboid migration as an alternative to mesenchymal migration in Matrigel. As all these effects can be reversed by pharmacological inhibition of ROCK, this suggests that $p27^{kip1}$ triggers macrophage mesenchymal migration by switching off amoeboid migration through inhibition of the Rho/ROCK pathway.

$p27^{kip1}$ relocation from the nucleus to the cytoplasm is required for macrophage mesenchymal migration

$p27^{kip1}$ is mainly recognised as a cell cycle regulator and is generally localised in nuclei (Sherr and Roberts, 1999), although other functions and cytoplasmic localisation have also been reported (Besson et al., 2006). In contrast, the Rho/ROCK signalling usually takes place in the cytoplasm, although nuclear localisation of RhoA (Shabo et al., 2008) and ROCK2 (Tanaka et al., 2006) have also been reported. So, we next investigated whether the role of $p27^{kip1}$ in macrophage 3D-migration is associated with its nuclear or cytoplasmic localisation.

We examined the intracellular localisation of $p27^{kip1}$ during macrophage 3D-migration. $p27^{kip1}$ phosphorylation on Ser10, although not sufficient for the nuclear to cytoplasmic redistribution of $p27^{kip1}$, is necessary for this process (Ishida et al., 2000; Kotake et al., 2005; Rodier et al., 2001). Therefore, pSer10-$p27^{kip1}$ can be present in both the cytoplasm and the nucleus, but the fraction of $p27^{kip1}$ which is effectively exported to the cytoplasm is necessarily phosphorylated on Ser10. We first performed western blot analysis of pSer10-$p27^{kip1}$ and total $p27^{kip1}$ in macrophages plated in 2D or migrating in 3D through fibrillar collagen, gelled collagen or Matrigel (Fig. 5A). The

Journal of Cell Science (2014) 127, 4009–4023 doi:10.1242/jcs.150987

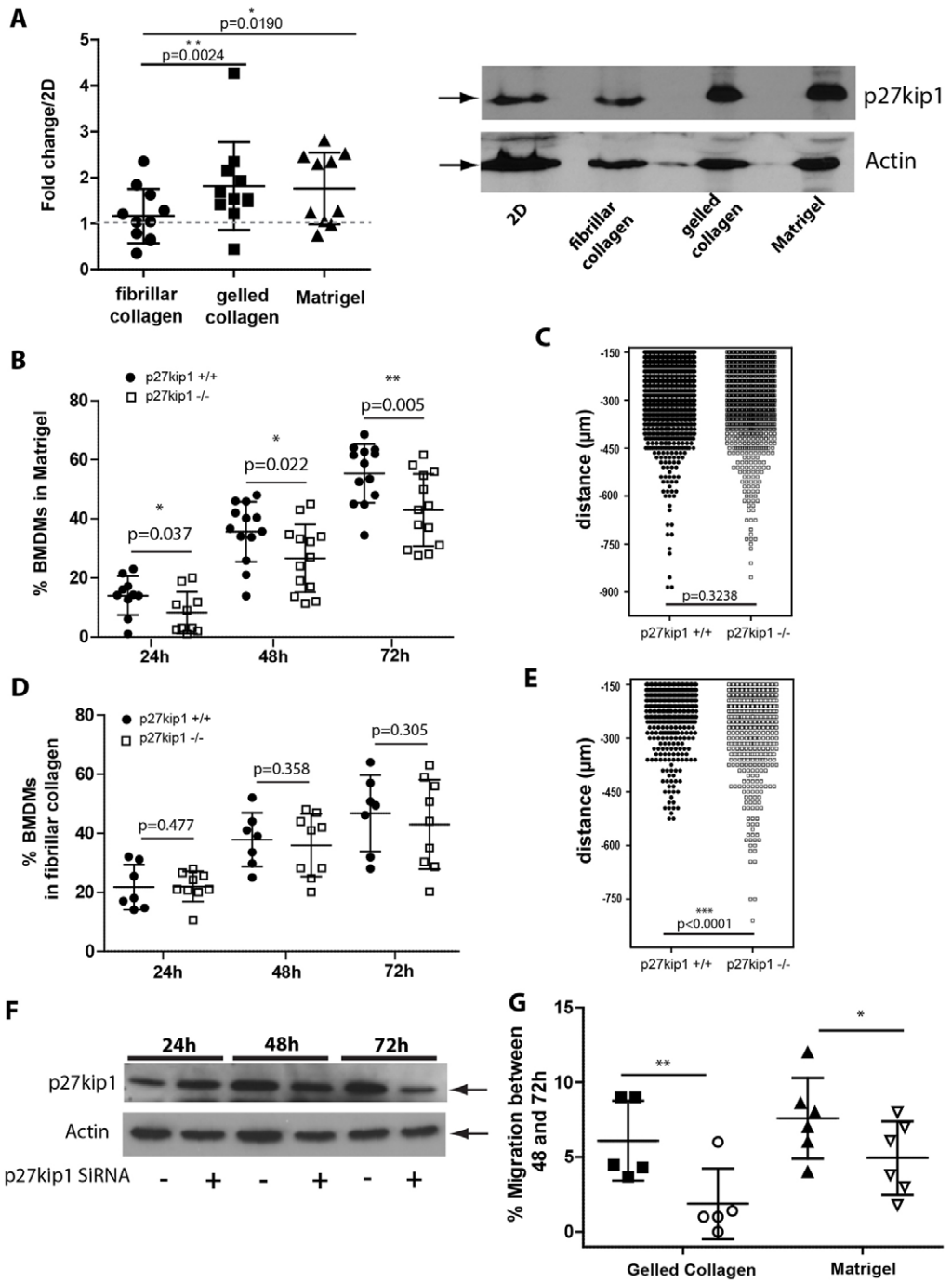

Fig. 3. p27^{kip1} promotes macrophage 3D-mesenchymal migration and reduces amoeboid migration efficiency. (A) p27^{kip1} is upregulated during macrophage mesenchymal but not amoeboid migration. Western blot analysis of p27^{kip1} expression levels in hMDMs from 10 independent donors in a 2D environment, and 3D Matrigel, fibrillar- and gelled collagen I following 72 h of migration. Fold changes compared to a 2D environment after normalisation to actin (loading control) are shown. A representative immunoblot is shown. Actin was used as a loading control. Statistics: two-tailed paired Student's *t*-test, 95% confidence interval (**P*=0.019; ***P*=0.0024). (B-E) p27^{kip1} deficiency inhibits triggering of macrophage mesenchymal migration and increases amoeboid migration efficiency. p27$^{kip1+/+}$ (black circles) and p27$^{kip1-/-}$ (white squares) BMDMs were allowed to migrate through Matrigel (B,C) or fibrillar collagen (D,E). The percentage of BMDM migration (B,D) and the *z*-distribution within the matrix (C,E) were measured. In the graph displaying the percentage of BMDM migration, each point represents an individual mouse (mean value of migration inserts performed in triplicate). The mean ± s.d. of 7–13 mice is shown. For the *z*-distribution, each point represents the *z*-position (µm) of a BMDM within thematrix (the surface of the matrix is at 0). The migration distances of 3126 and 688 p27$^{kip1+/+}$ BMDMs and 2806 and 945 p27$^{kip1-/-}$ BMDMs (from 3-5 mice) were measured in Matrigel (C) and in fibrillar collagen (E), respectively. Statistics: unpaired Student's *t*-test, two-tailed, 99% confidence interval; *P*=0.010 (B), *P*=0.3238 (C), *P*=0.477 (D), *P*<0.0001 (E). (F,G) p27^{kip1} silencing in hMDMs affects mesenchymal migration. (F) p27^{kip1} depletion in control or p27^{kip1} siRNA-transfected hMDMs was monitored by western blotting at 24, 48 or 72 h post-transfection. One representative experiment is shown. (G) hMDMs transfected with a control siRNA (dark) or p27^{kip1} siRNA (white) were loaded on top of thick layers of gelled-collagen I or Matrigel immediately after transfection. Cell migration was monitored at 24, 48 and 72 h, and the percentage of migrating cells was measured. The results are expressed as the percentage of cell migration between 48 and 72 h when p27^{kip1} silencing was efficient. Each point represents one independent blood donor (mean value of migration inserts performed in triplicates). The mean ± s.d. of five to six independent donors is shown. Statistics: paired Student's *t*-test, one-tailed, 99% confidence interval (***P*=0.0067, **P*=0.018).

Journal of Cell Science

Journal of Cell Science (2014) 127, 4009–4023 doi:10.1242/jcs.150987

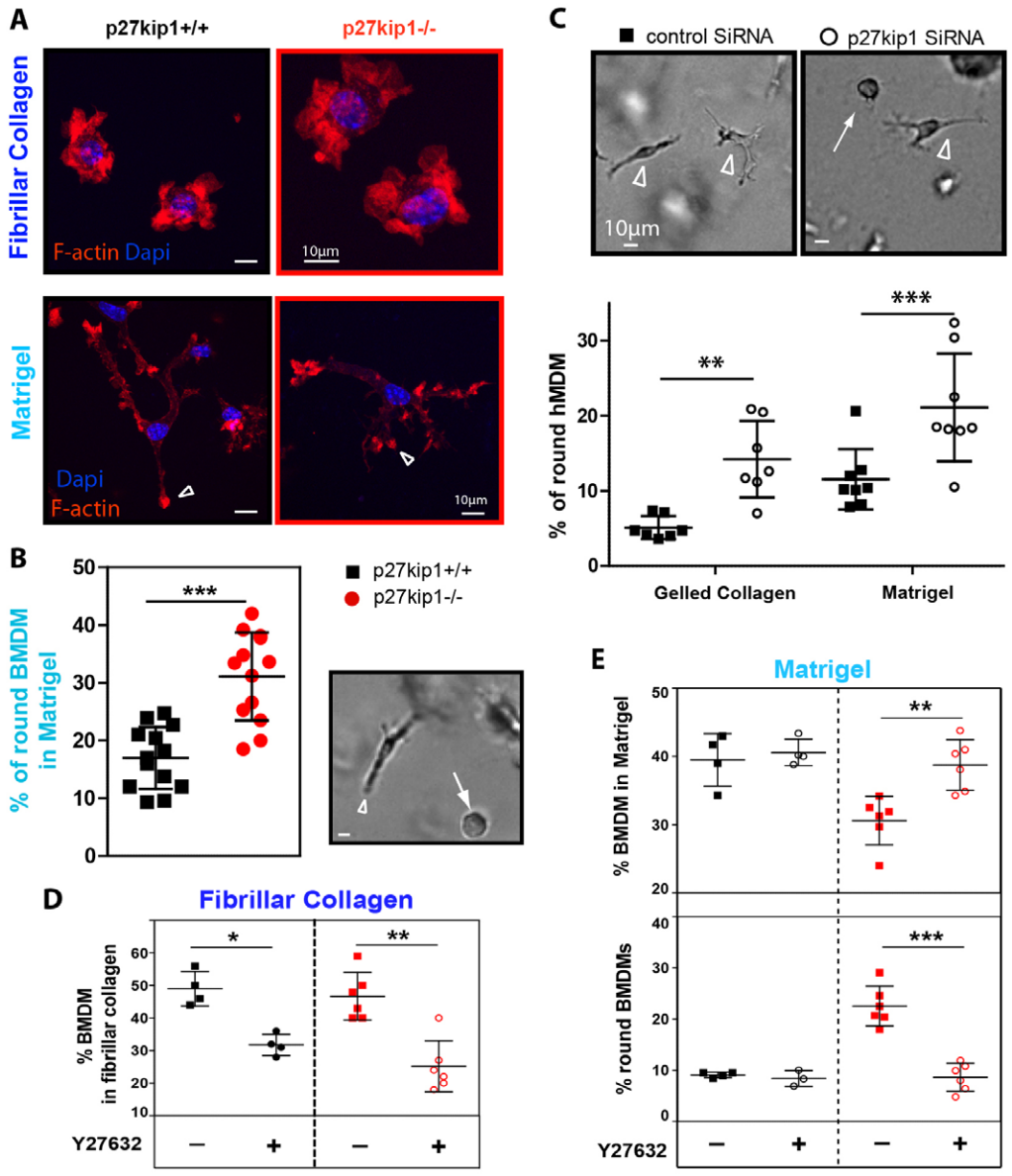

Fig. 4. p27^{kip1} deficiency promotes amoeboid migration instead of mesenchymal migration in dense matrices and is counterbalanced by ROCK inhibition. (A,B) The morphology of p27$^{kip1+/+}$ (black) and p27$^{kip1-/-}$ (red) BMDMs in matrices was observed by confocal microscopy following F-actin (phalloidin–Texas-Red) and DAPI staining (A) and brightfield transmission microscopy (B). Representative images are shown. Arrowheads in A indicate F-actin-rich 3D-podosomes. Elongated (B, arrowheads) and round (B, arrow) BMDMs were counted after 72 h of migration, and the percentage of round BMDMs within Matrigel was calculated (B, graph). Each point represents an individual mouse (mean value of migration inserts performed in triplicate). The mean ± s.d. of 12 to 13 mice is shown. Statistics: unpaired Student's *t*-test, one-tailed, 99% confidence interval; $P<0.0001$ (B). (C) p27^{kip1} silencing in hMDMs induces a shift from an elongated to a round phenotype. hMDMs transfected with control siRNA (dark) or p27^{kip1} siRNA (white) were loaded on top of thick layers of gelled-collagen or Matrigel immediately after transfection. The morphology of hMDMs in matrices was observed by using phase contrast microscopy, and elongated (arrowheads) and round (arrow) hMDMs were counted after 72 h of migration. The results are expressed as the percentage of round hMDMs in the matrices. Each point represents one independent blood donor (mean value of migration inserts performed in triplicates). The mean ± s.d. of seven independent donors is shown. Statistics: Paired Student's *t*-test, one-tailed, 99% confidence interval (**P=0.002, ***P=0.001). (D,E) The percentage of migrating p27$^{kip1+/+}$ (black) and p27$^{kip1-/-}$ (red) BMDMs and the percentage of round BMDMs were measured for untreated (−) or Y27632 (10 µM)-treated (+) cells migrating within fibrillar collagen (D) and Matrigel (E). Statistics: paired Student's *t*-test, two-tailed, 95% confidence interval; *P=0.011, **P=0.001 (D); **P=0.001, ***P=0.0007 (E). In E, differences between untreated and Y27632-treated p27$^{kip1+/+}$ BMDMs were not significant (P=0.613 top panel and P=0.173 bottom panel).

pSer10-p27^{kip1} to p27^{kip1} ratio was increased in macrophages migrating through gelled collagen and Matrigel compared to those migrating through fibrillar collagen, indicating that the pool of p27^{kip1} that can be exported to the cytoplasm is increased during mesenchymal migration compared to amoeboid migration. Immunofluorescence analysis of macrophages in 3D matrices showed that pSer10-p27^{kip1} was mainly localised in the cytoplasm of hMDMs during mesenchymal migration (Fig. 5B, arrows), whereas it was concentrated into the nucleus during amoeboid migration (Fig. 5B, arrowheads). A significant decrease in the nuclear-to-cytoplasmic signal ratio of pSer10-p27^{kip1} was calculated in mesenchymal hMDMs compared to amoeboid hMDMs (Fig. 5C). This indicated that macrophage mesenchymal migration is correlated with the

Journal of Cell Science (2014) 127, 4009–4023 doi:10.1242/jcs.150987

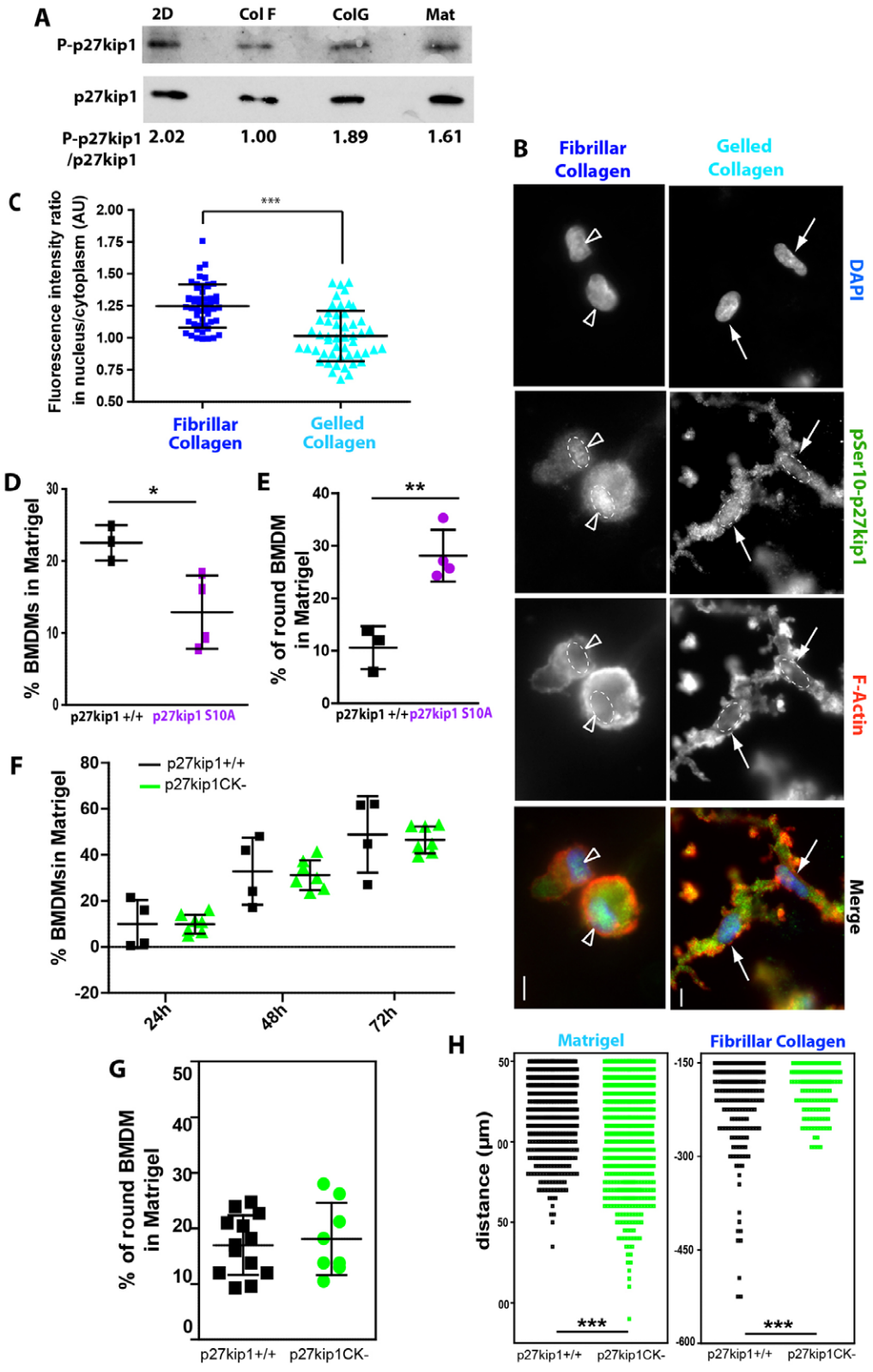

Fig. 5. See next page for legend.

phosphorylation-dependent relocation of $p27^{kip1}$ from the nucleus to the cytoplasm.

Next, we used BMDMs from mutant mice that each express a mutant of $p27^{kip1}$ protein that is known to mislocalise. The first type of mutant BMDMs, expresses $p27^{kip1}$ of which Ser10 is mutated to Ala, yielding mutant protein $p27^{kip1}$Ser10Ala (Besson et al., 2006). In $p27^{kip1}$Ser10Ala mice, total expression level of $p27^{kip1}$Ser10Ala in macrophages is reduced compared to

Journal of Cell Science (2014) 127, 4009–4023 doi:10.1242/jcs.150987

Fig. 5. $p27^{kip1}$ promotes 3D-mesenchymal migration in a way dependent on its phosphorylation and its relocation from the nucleus to the cytoplasm. (A) The relative amount of pSer10-$p27^{kip1}$ (P-p27kip1) is increased during macrophage mesenchymal migration. Western blot analysis of pSer10-$p27^{kip1}$ level in parallel to $p27^{kip1}$ expression levels was performed in hMDMs in a 2D environment, and 3D Matrigel, fibrillar- and gelled collagen following 72 h of migration. Ratio of pSer10-p27kip1 to total p27kip1 signal was calculated. Experiments were performed on hMDMs isolated from three independent donors and one representative experiment is shown. (B,C) $p27^{kip1}$ (pSer10-p27kip1) is exported to the cytoplasm during macrophage mesenchymal migration. After 72 h of migration, hMDMs in 3D matrices (fibrillar- or gelled collagen) were fixed, permeabilised and stained with antibody against phosphorylated Ser10 in $p27^{kip1}$, phalloidin–Texas-Red for F-actin and DAPI for nuclei. (B) Representative images obtained by epifluorescence acquisition are shown. Scale bars: 10 µm. Cells that are out of focus are macrophages inside the matrix that are either above or below the hMDMs which in focus. The cytoplasmic localisation of $p27^{kip1}$ and the lack of nuclear labelling in gelled collagen are indicated by arrows. Nuclear accumulation of $p27^{kip1}$ is indicated by arrowheads. Nuclei are surrounded by dashed lines. Fluorescence intensities were measured and ratios between the nucleus and cytoplasm (C) were calculated in at least 50 hMDMs during five independent experiments (mean±s.d.). Statistics: paired Student's *t*-test, two-tailed, 95% confidence interval, $P<0.0001$ (B). (D,E) The $p27^{kip1}$Ser10Ala (p27kip1 S10A) mutant has a nuclear export defect and leads to an impaired triggering of macrophage mesenchymal migration. $p27^{kip1+/+}$ (black) and $p27^{kip1}$Ser10Ala (purple) BMDMs were allowed to migrate through Matrigel. The percentage of cell migration (D) and the number of round BMDMs (E) were quantified. Each point represents an individual mouse (mean value of migration inserts performed in triplicates). Mean ± s.d. of three to four mice are shown. Statistics: unpaired student *t*-test, two-tailed, 99% confidence interval. $P=0.0154$ (D), $P=0.002$ (E). (F–H) The cytoplasmic localisation of $p27^{kip1}$CK- correlates with enhanced mesenchymal and diminished amoeboid migration. $p27^{kip1+/+}$ (black) and $p27^{kip1}$CK- (green) BMDMs were allowed to migrate through Matrigel (F–H) or fibrillar collagen (H). The percentage of BMDM migration (F), the percentage of round BMDMs (G) and the *z*-distribution within the matrices (H) were measured. In F and G, each point represents an individual mouse (mean value of migration performed in triplicates). The mean ± s.d. of at least four mice is shown. In H, each point represents the *z*-position (µm) of a BMDM within the matrix (0 representing the surface of the matrix). A total of 763 and 232 BMDMs from three $p27^{kip1+/+}$ mice and 1470 and 170 from three $p27^{kip1}$CK- mice were analysed in Matrigel and fibrillar collagen, respectively. Statistics: unpaired Student's *t*-test, two-tailed, 99% confidence interval. $P=0.50$ at 24 h, $P=0.40$ at 48 h and $P=0.37$ at 72 h (F), $P=0.67$ (G), $P<0.0001$ (H).

$p27^{kip1+/+}$ macrophages, but its nuclear localisation is increased (Fuster et al., 2011). The percentage of migration of $p27^{kip1}$Ser10Ala BMDMs inside Matrigel was reduced by 43% ± 5 at 24 h compared to $p27^{kip1+/+}$ cells (Fig. 5D), and the percentage of round cells was increased (Fig. 5E) showing that, in Matrigel, mesenchymal migration triggering was reduced similarly to $p27^{kip1}$-deficient macrophages and amoeboid migration was equally stimulated. Again, the migration distance of $p27^{kip1}$Ser10Ala BMDMs that could still migrate was unchanged compared to wild-type cells (data not shown), suggesting that a defect in $p27^{kip1}$ nuclear export correlates with reduced mesenchymal migration triggering but not migration efficiency.

The second type of mutant BMDMs originated from $p27^{kip1}CK^-$ knock-in mice that carry point mutations in the cyclin- and CDK-binding domains of $p27^{kip1}$. The expressed mutant protein has lost its cell cycle functions (Besson et al., 2006; Vlach et al., 1997) and its quantity in the cytoplasm is increased in resting cells compared to wild-type $p27^{kip1}$ (Serres et al., 2011). In addition, $p27^{kip1}CK^-$ knock-in mice have increased overall expression levels of the mutant protein compared to the level of $p27^{kip1}$ observed in wild-type mice (Besson et al., 2006). We found that a similar percentage of $p27^{kip1}CK^-$ BMDMs migrated within Matrigel compared to $p27^{kip1+/+}$ BMDMs, even at longer migration times (Fig. 5F); and the percentage of round BMDMs was not affected (Fig. 5G). Interestingly, as shown on Fig. 5H, the migration distances of $p27^{kip1}CK^-$ BMDMs were significantly increased in Matrigel and reduced in fibrillar collagen. This further demonstrates that the effect of $p27^{kip1}$ on 3D-migration is correlated with its cytoplasmic localisation and shows that potentiation of mesenchymal migration is correlated with diminished amoeboid migration efficiency. We conclude from these observations that the role of $p27^{kip1}$ in triggering mesenchymal migration is correlated with its export from the nucleus to the cytoplasm.

Tissue recruitment of macrophages is dependent on the cytoplasmic localisation of $p27^{kip1}$

Finally, to determine the role of $p27^{kip1}$ in macrophage tissue infiltration *in vivo*, we compared macrophage recruitment into tumours that had been induced in $p27^{kip1-/-}$ and $p27^{kip1}CK^-$ mice. In these two mice genotypes, the cell cycle activity of $p27^{kip1}$ is abolished; it is intact in $p27^{kip1+/+}$ mice. Consequently, $p27^{kip1-/-}$ and $p27^{kip1}CK^-$ mice are phenotypically very close to each other and very distant to $p27^{kip1+/+}$ mice: they both develop hyperplasia of several organs, and are taller and bigger than $p27^{kip1+/+}$ mice (Besson et al., 2007; Fero et al., 1996). Experiments were also performed on wild-type mice but we decided to compare the two genotypes devoid of $p27^{kip1}$ cell cycle activity as a priority to avoid bias.

Urethane is a potent carcinogen that induces lung tumours in mice that are frequently infiltrated with macrophages (Ishigami et al., 2011; Serres et al., 2011). We used previously described lung tissues from urethane-treated $p27^{kip1-/-}$ and $p27^{kip1}CK^-$ mouse cohorts to carry out F4/80 labelling to stain macrophages (Serres et al., 2011). Interestingly, macrophage recruitment in lung tumours and the surrounding tissue was markedly reduced in $p27^{kip1-/-}$ mice compared to $p27^{kip1}CK^-$ mice (Fig. 6A,B). In wild-type mice, the number of F4/80-positive cells in surrounding healthy tissue was comparable to $p27^{kip1-/-}$ mice and lower than in $p27^{kip1}CK^-$ mice (Fig. 7). The number of macrophages recruited into lung tumours was equally increased in $p27^{kip1+/+}$ and $p27^{kip1}CK^-$ mice compared to $p27^{kip1-/-}$ mice (Fig. 7). These differences could not be attributed to a higher number of circulating monocytes in $p27^{kip1}CK^-$ mice, as the percentages of circulating monocytes in $p27^{kip1-/-}$, $p27^{kip1}CK^-$ and $p27^{kip1+/+}$ mice were 9.61% ± 4.18, 11.45% ± 1.06 and 8.95% ± 3.80, respectively (mean ± s.d. of three mice). The subcellular localisation of $p27^{kip1}CK^-$ was mainly cytosolic in tissue macrophages, which is in marked contrast to its nuclear accumulation in F4/80-negative, SPC-positive cells (Fig. 6C,D).

We conclude that, *in vivo*, the tissue recruitment of macrophages is controlled by $p27^{kip1}$ that accumulates in their cytoplasm, thus corroborating our *in vitro* data. In addition, our results suggest that part of the migration process towards tumour tissues involves mesenchymal motility, as we have previously shown that this mode of migration is hindered by $p27^{kip1}$ deficiency.

DISCUSSION

Characterisation of macrophage 3D-migration represents a challenging research field that could potentially provide pharmacological tools for the control of the deleterious tissue

Journal of Cell Science (2014) 127, 4009–4023 doi:10.1242/jcs.150987

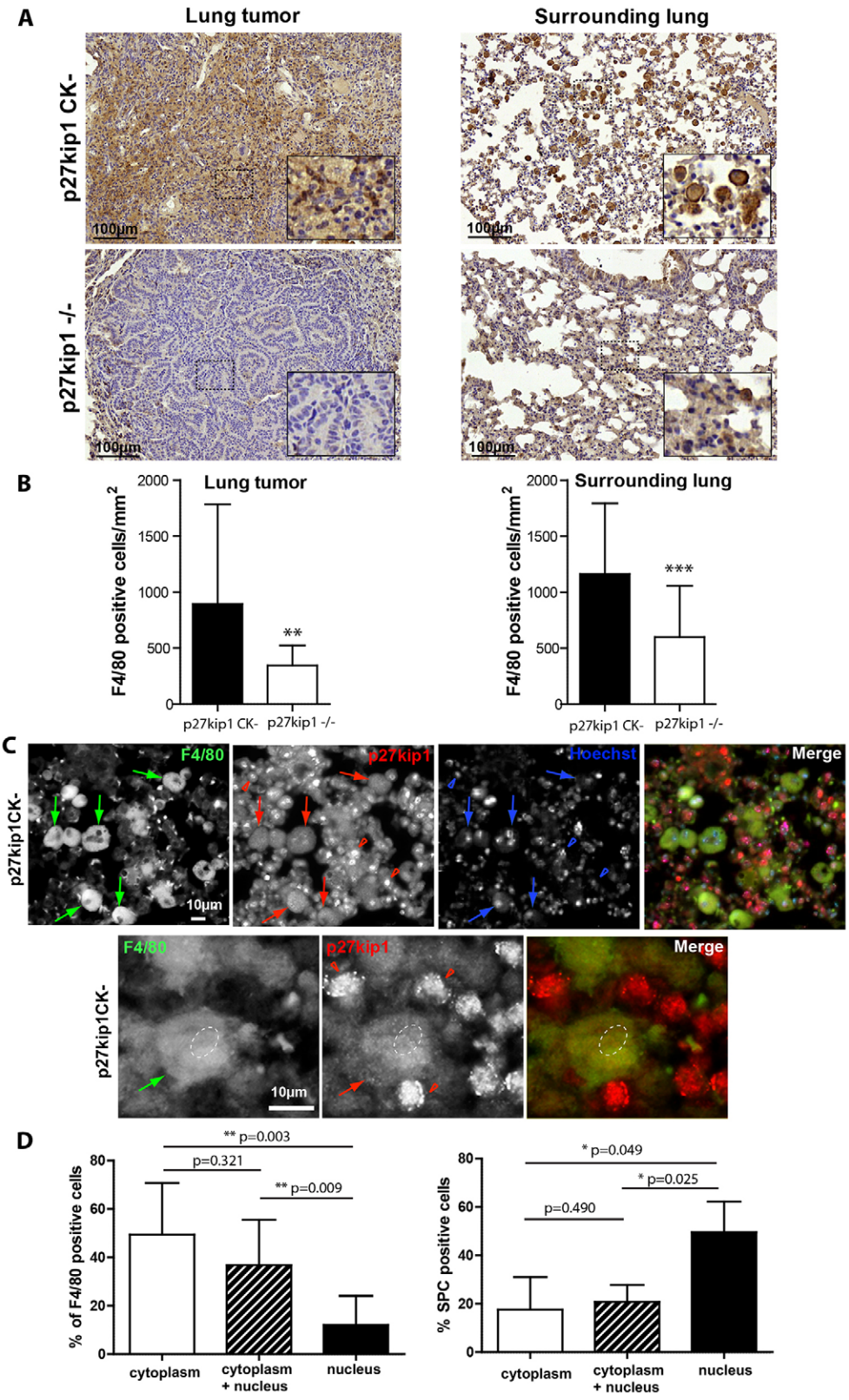

Fig. 6. The recruitment of macrophages into lung tumours is dependent on p27^{kip1} localised to the cytoplasm. Lung sections of urethane-treated p27$^{kip1-/-}$ and p27^{kip1}CK- mice were prepared and labelled. (A) Lung tumours (left) and surrounding healthy tissues (right) immunohistochemistry sections stained with anti-F4/80 antibody to evaluate macrophage tissue infiltration. (B) Quantification of F4/80-positive cells per mm^2 of lung tumor (left) and surrounding healthy tissue (right). Statistics: One-way ANOVA: $^{**}P=0.006$, $^{***}P<0.0001$. (C) Lung tumour immunohistochemistry sections labelled with anti-F4/80 (macrophages, green), anti-p27^{kip1} (red), anti-SP-C antibodies (alveolar type II and adenocarcinoma cells, purple) and Hoechst 33304 (nuclei, blue) to assess cytoplasmic localisation of p27^{kip1}. A higher magnification of lung slices from p27^{kip1}CK- mice is also shown. Arrows indicate macrophages with cytoplasmic localisation of p27^{kip1}, and arrowheads indicate adjacent F4/80-negative cells showing nuclear localisation of p27^{kip1}. Hoechst staining was used to define nuclei position (not shown on bottom pictures but replaced by a dashed circle for clarity). (D) Quantification of the proportion of F4/80-positive cells (left graph) or F4/80-negative cells (right graph: SPC positive cells) with cytoplasmic and/or nuclear localisation of p27^{kip1}. Statistics: paired Student's *t*-test, two-tailed, 95% confidence interval.

infiltration of these cells in inflammatory diseases and cancers. Macrophages are the only leukocytes known to adopt a mesenchymal mode when migrating through dense matrices (Cougoule et al., 2012; Van Goethem et al., 2010). Our existing findings on macrophage mesenchymal migration are based on the formation and organisation of podosomes, which are implicated in ECM proteolysis (Cougoule et al., 2010; Guiet et al., 2012; Van Goethem et al., 2011; Van Goethem et al., 2010). In the present study, we uncover another mechanism regulating macrophage mesenchymal migration, based on the finding that a single macrophage is equipped to employ both amoeboid and mesenchymal migration, and that hindering of amoeboid

Journal of Cell Science

Journal of Cell Science (2014) 127, 4009–4023 doi:10.1242/jcs.150987

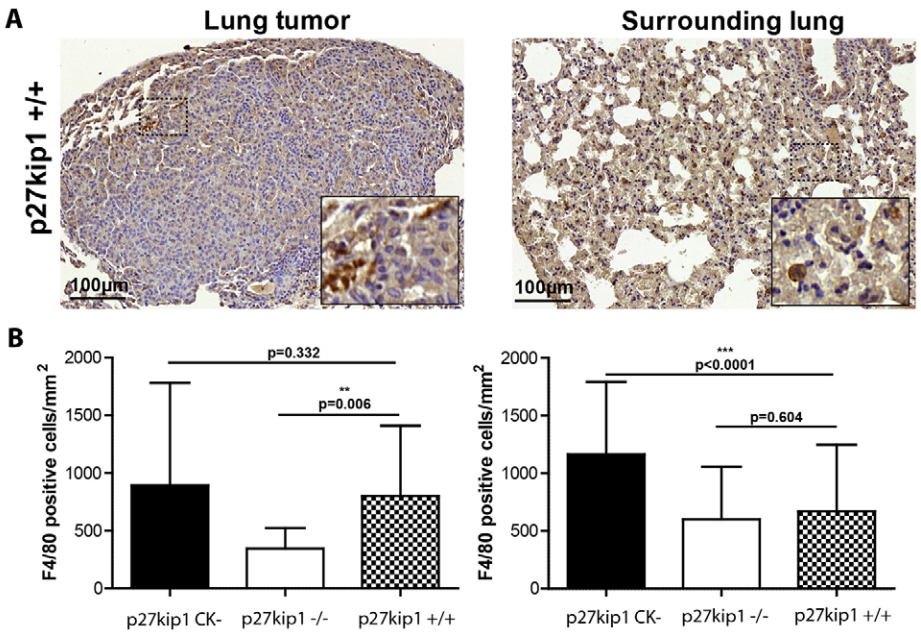

Fig. 7. The recruitment of macrophages into lung tumours is equally increased in $p27^{kip1+/+}$ and $p27^{kip1}CK^{-}$ mice compared to $p27^{kip1-/-}$ mice. (A) Lung tumour and surrounding healthy tissue immunohistochemistry sections from $p27^{kip1+/+}$ mice stained with anti-F4/80 antibody to evaluate macrophage tissue infiltration. (B) Quantification of F4/80-positive cells per mm^2 of tissue from $p27^{kip1+/+}$ is compared to the quantifications obtained on $p27^{kip1-/-}$ and $p27^{kip1}$CK- mice (presented in Fig. 6). Statistics: One-way ANOVA.

migration through inhibition of the Rho/ROCK pathway participates in mesenchymal migration triggering (Fig. 8).

The present findings suggest that RhoA inhibition is a requisite for switching off amoeboid migration, thus prompting cells to use mesenchymal migration in dense matrices. Rho-GTPases have largely been involved in the remodelling of actin-cytoskeleton during cell migration (Sahai and Marshall, 2003). In tumour cell lines, activation of Rho-ROCK signalling is necessary to promote the round morphology with bleb-like structures characteristic of amoeboid migration, and to antagonise the formation of elongated protrusions (Sahai and Marshall, 2003). In line with this, we observed that ROCK inhibition induces a change in macrophage morphology both on the surface and inside Matrigel: macrophages become even more elongated and protrusive after treatment with inhibitor Y27632 compared to untreated cells. We, therefore, propose that macrophages exhibiting this protrusive phenotype are more prone to worm their way into the small holes that they create by proteolysis in a dense matrix during mesenchymal migration. In contrast, the triggering of macrophage mesenchymal migration in fibrillar collagen upon amoeboid migration inhibition was not observed. Indeed, we have clearly shown that ROCK inhibition completely abolishes macrophage migration through fibrillar collagen. One explanation could be that – in contrast to tumour cells such as HT1080, which can employ mesenchymal migration in either loose or dense matrices (Carragher, 2006; Friedl and Wolf, 2003) – amoeboid migration is the default migration mode of macrophages in fibrillar collagen, whereas mesenchymal migration is only triggered by the contact of macrophages with dense matrices and could require additional effectors that are not expressed during amoeboid migration or upon macrophage contact with loose matrices. So, although ROCK inhibition induces an elongated macrophage morphology, this is not sufficient to trigger macrophage mesenchymal migration in fibrillar collagen.

Since amoeboid migration inhibition is likely to participate in the triggering of mesenchymal migration in dense matrices, we considered whether mesenchymal migration inhibition conversely participates in amoeboid migration triggering in loose matrices. However, this seems unlikely because we have never observed any evidence of amoeboid migration activation in macrophages migrating through fibrillar collagen by using pharmacological inhibitors of mesenchymal migration, such as protease inhibitors (Van Goethem et al., 2010).

In this present work, we propose that $p27^{kip1}$ is an upstream trigger of inhibition of the Rho/ROCK pathway during macrophage mesenchymal migration. Until recently, $p27^{kip1}$ was mainly recognised as an inhibitor of the cell cycle as it prevents the activation of cyclin–CDK complexes and, thus, negatively controls cell proliferation by arresting the cell cycle at the G1/S transition (Besson et al., 2004a; Sherr and Roberts, 1999). However, $p27^{kip1}$ has also been shown to participate in the migration of cancer cells (Denicourt et al., 2007; Nagahara et al., 1998), mouse fibroblasts (Besson et al., 2004b) and neuronal progenitor cells (Kawauchi et al., 2006; Ueno et al., 2011), but its function in cell migration is quite conflicting depending on the cellular context. Cytoplasmic $p27^{kip1}$ has been reported to interact with stathmin (a microtubule-destabilising protein) in Src-transformed fibroblasts and RhoA in primary fibroblasts to inhibit and stimulate cell migration, respectively (Baldassarre et al., 2005; Besson et al., 2004b). Our results contribute to consolidate pro- and anti-migratory functions of $p27^{kip1}$ because we show here that $p27^{kip1}$ is pro-migratory regarding mesenchymal migration but is anti-migratory regarding amoeboid migration.

We report for the first time $p27^{kip1}$ upregulation during mesenchymal migration and not amoeboid migration, and this is correlated with the upregulation of the corresponding mRNA (data not shown). We propose that this upregulation participates in the potentiation of mesenchymal migration based on our observation that mesenchymal migration is affected in $p27^{kip1}$-mutant BMDMs.

Among the potential partners of $p27^{kip1}$, our results support a causal relationship between the inhibition of the RhoA signalling pathway, the regulation of mesenchymal migration and $p27^{kip1}$ because (i) phosphorylation of markers of the Rho/ROCK pathway activity is diminished during mesenchymal migration

Journal of Cell Science (2014) 127, 4009–4023 doi:10.1242/jcs.150987

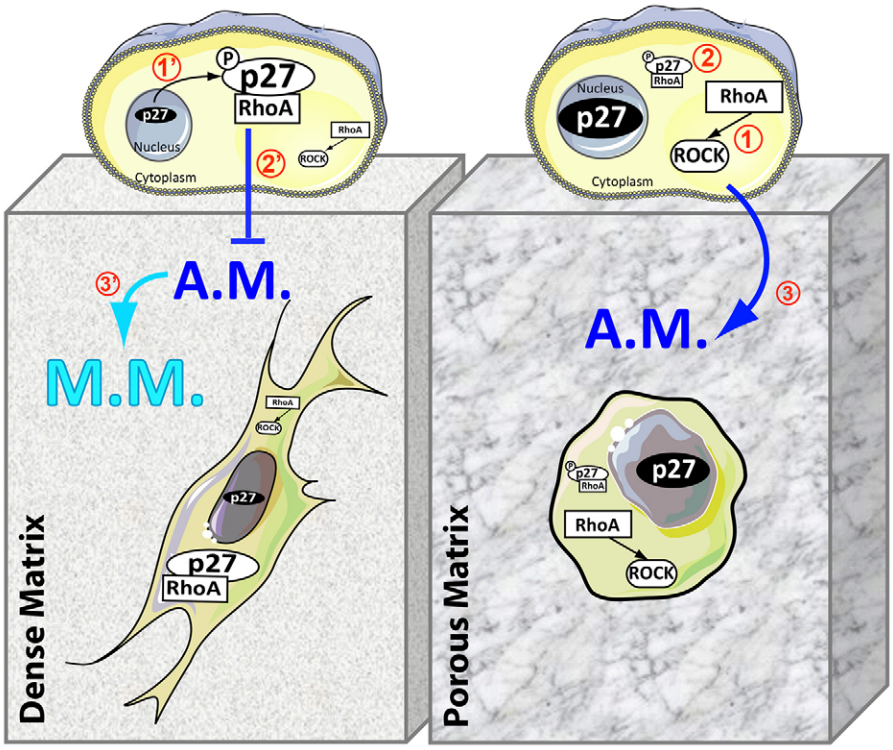

Fig. 8. Proposed model of the regulation of macrophage 3D-migration by p27^{kip1}. When adhering to a porous matrix (right panel), p27^{kip1} status is unchanged compared to its status in 2D (dense matrix). p27^{kip1} expression levels are not increased and remain mostly in macrophage nuclei. Therefore p27^{kip1} does not significantly interfere with the Rho/ROCK signalling pathway (1) which is likely to activate amoeboid migration by generating a ROCK-mediated actomyosin contractile force (3). It is worth noting that in wild-type macrophages a small proportion of p27^{kip1} is present in the cytoplasm and might neutralise part of the cytoplasmic RhoA, therefore restricting full amoeboid migration efficiency (2). This might explain why amoeboid migration efficiency is increased in p27$^{kip1-/-}$ and p27^{kip1}Ser10Ala macrophages. In contrast, upon adhesion on dense matrices (left panel), p27^{kip1} expression levels are increased and the protein is exported from the nucleus to the cytoplasm in a phosphorylation-dependent manner (1′). This induces neutralisation of cytoplasmic RhoA (Besson et al., 2004b) (2′) which can no longer activate the ROCK signalling pathway required for amoeboid migration. Consequently, this leads to inhibition of amoeboid migration, which is likely to participate in the triggering of mesenchymal migration (3′). This process is exacerbated in the p27^{kip1}CK^{-} mutant, in which the proportion of cytoplasmic p27^{kip1} is increased compared to wild-type, leading to a more-efficient mesenchymal migration.

and pharmacological inhibition of this pathway activates macrophage mesenchymal migration and, (ii) the ROCK inhibitor Y27632 reverses the effect of p27^{kip1} deficiency on mesenchymal migration. In addition, we show that activation of mesenchymal migration correlates with p27^{kip1} relocation to the cytoplasm, where it is more prone to interact with RhoA. In contrast, during migration through porous matrices, such as fibrillar collagen, p27^{kip1} is neither upregulated nor relocated to the cytoplasm, thus limiting its interference with RhoA as proposed in Fig. 8.

In addition to reduced mesenchymal migration observed in Matrigel, we report that p27^{kip1} deficiency induces partial activation of amoeboid migration, with ~30% of p27$^{kip1-/-}$ BMDMs exhibiting the round amoeboid-like cell shape. Although we have never – as described for tumour cells (Carragher et al., 2006; Friedl and Wolf, 2003; Sahai and Marshall, 2003) – observed a clear mesenchymal–amoeboid transition with macrophages, this observation suggests that, although not complete, partial transition from mesenchymal to amoeboid migration could occur in Matrigel despite its low porosity. This p27$^{kip1-/-}$ BMDM phenotype can be reversed by ROCK inhibition, further supporting a shift from mesenchymal to amoeboid migration. This result was quite surprising in a dense matrix, whose porosity is too low to allow cells to migrate without previous proteolysis. We have previously shown that macrophages create tunnel-like pathways when progressing into low-porosity matrices such as Matrigel, requiring proteolytic remodelling in order to be infiltrated (Guiet et al., 2011; Van Goethem et al., 2011; Van Goethem et al., 2010). These tunnels can be used by trailing round macrophages (Guiet et al., 2011; Van Goethem et al., 2011; Van Goethem et al., 2010). We propose that, in the absence of p27^{kip1}, BMDMs show a propensity to shift back to non-proteolytic amoeboid migration and migrate using the tunnel-like pathways created by forerunner mesenchymal migrating cells.

Tissue infiltration of macrophages into tumours generally favours tumour growth and invasiveness (Pollard, 2009; Porta et al., 2011), and p27^{kip1} has been shown to be oncogenic (Besson et al., 2007). We show that cytoplasmic p27^{kip1} is required for efficient tumour infiltration by macrophages. We propose that p27^{kip1} achieves this pathophysiological role by stimulating mesenchymal migration of macrophages. Interestingly, in contrast to p27$^{kip1-/-}$ mice, aging p27^{kip1}CK^{-} mice spontaneously develop lung tumours that are infiltrated by macrophages and are locally invasive (Besson et al., 2007). Therefore, macrophages that are competent to employ mesenchymal migration seem to display a greater ability to infiltrate of lung tumours.

This work uncovers p27^{kip1} as a new effector of macrophage 3D-migration, which promotes mesenchymal migration at least partly through inhibition of amoeboid migration. Interestingly, it

also controls tissue infiltration of macrophages in a tumour model, suggesting that targeting an effector of mesenchymal migration is a relevant therapeutic strategy for reducing the presence of macrophages in pathologic tissues.

MATERIALS AND METHODS

Isolation of monocytes and culture of hMDMs and BMDMs

$p27^{kip1+/+}$, $p27^{kip1-/-}$, $p27^{kip1}$Ser10Ala and $p27^{kip1}CK^{-}$ mice have been previously described (Biswas et al., 2006; Fero et al., 1996). Human monocytes were isolated from blood of healthy donors (buffy coat obtained from Etablissement Français du Sang, Toulouse, France) and differentiated into human monocyte-derived macrophages (hMDMs) as previously described (Van Goethem et al., 2010). Blood samples were obtained following standard ethical procedures and with the approval of the concerned Internal Review Boards.

Bone-marrow-derived macrophages (BMDMs) were isolated from $p27kip1^{+/+}$, $p27kip1^{-/-}$, p27kip1Ser10Ala and $p27kip1CK^{-}$ mice and BMDMs were prepared as previously described (Cougoule et al., 2010). All experiments were performed according to animal protocols approved by the Animal Care and Use committee of the Institut de Pharmacologie et de Biologie Structurale.

Extracellular matrix preparation and 3D-migration assay

Fibrillar collagen I, gelled collagen I and Matrigel were prepared as described previously (Van Goethem et al., 2010), except that Nutragen (Advanced BioMatrix, San Diego, CA) was mixed with rat tail collagen I (BD Biosciences, Le Pont de Claix, France) (1 mg/ml final collagen concentration) for fibrillar collagen. Pepsin-extracted denatured collagen was used instead of native collagen because the latter only allows polymerisation into dense gel and, therefore, can only generate MM in macrophages (Van Goethem et al., 2010; Wiesner et al., 2014). Matrices (100 µl) were polymerised in Transwell Invasion Chambers (BD Falcon, Le Pont de Claix, France) placed within 24-well Companion plates (BD Biosciences). 3D migration assays with or without ROCK inhibitor Y27632 were performed as described (Van Goethem et al., 2010). Only Matrigel was used in BMDM migration assays to trigger mesenchymal migration because, in contrast to hMDMs, these cells are unable to migrate through gelled collagen (Cougoule et al., 2010). Migration experiments were conducted for 24–72 h and the percentage of cell migration, the morphology of migrating macrophages and the distance of migration were monitored as described (Van Goethem et al., 2010).

siRNA transfection of hMDMs

hMDMs were transfected with small interfering RNA (siRNA) (sequence information available from the authors on request) by electroporation using the Neon® Transfection System (Invitrogen, Saint-Aubin, France). A pellet of 2×10^5 harvested hMDMs per transfection was obtained by centrifugation and resuspended in 10 µl of R buffer [containing 75 nmol of either control non-targeting or $p27^{kip1}$ siRNA (Dharmacon RNA Technologies, Thermo Scientific, Illkirch, France)]. Cells were then electroporated with two 40-ms pulses of 1000 V, immediately transferred to a tube with complete medium and seeded on glass coverslips for further western blot analysis or on 3D matrices polymerised in Transwell inserts for migration assays. Knockdown of $p27^{kip1}$ was assessed 24 h, 48 h and 72 h post-transfection by western blot analysis on transfected macrophages loaded on glass coverslips.

Western blotting

Protein extracts were obtained by homogenising cells adhering to glass coverslips or migrating in 3D ECMs in boiling Laemmli cell lysis buffer (1× for 2D and 4× for 3D) until complete dissolution of the matrix. We used primary rabbit anti-$p27^{kip1}$ polyclonal antibodies (1:1000; Cell Signaling), rabbit anti-phosphoSer10-$p27^{kip1}$ monoclonal antibodies (1:500; Abcam, Cambridge UK), rabbit anti-cofilin (1:100; Cell Signaling), rabbit anti-phospho-Ser3-cofilin (1:1000; Cell Signaling), rabbit anti-ERM (1:100; Cell Signaling) and anti-phospho-ERM (1:1000; Cell Signaling) for 16h at 4℃ followed by secondary goat anti-rabbit immunoglobulin G antibodies coupled to horseradish peroxidase (1:10,000; BioRad, Marnes-la-Coquette, France) for 2h at room temperature. Rabbit anti-actin primary antibody (1:10,000; Sigma-Aldrich) was used as loading control. The quantification of western blots was conducted using Image J software and values were normalised to the loading control.

Immunostaining and fluorescent microscopy

Cells on glass coverslips or in matrices were fixed and stained as previously described (Van Goethem et al., 2011; Van Goethem et al., 2010). For $p27^{kip1}$ localisation, cells were stained with primary antibody for 48h, either rabbit anti-$p27^{kip1}$ (1:1000; Ozyme, Cell Signaling, St-Quentin-En-Yvelines, France) or rabbit anti-P-Ser10-$p27^{kip1}$ (1:100; BD Biosciences), followed by an anti-mouse or anti-rabbit secondary antibody conjugated to Alex-Fluor-488 (1:500 or 1:1000, respectively; Cell Signaling), DAPI (1:750; Sigma-Aldrich, Lyon, France) and phalloidin–Texas-Red (1:200; Molecular Probes, Invitrogen) for 2h. Images were acquired using a DM-RB fluorescence microscope (Leica Microsystems, Deerfield, IL) or a confocal FV1000 microscope (Olympus, Hamburg, Germany). The same exposure times were used when images had to be compared. All of the images were prepared with Adobe Photoshop®. Fluorescence intensity in circular areas of constant size was measured using Image J software and fluorescence intensity ratio in nucleus over cytoplasm (Arbitrary Units) was calculated for each macrophage. Statistical analysis was performed with GraphPad Prism software.

Immunohistochemistry and immunofluorescence on lung sections

Paraffin-embedded lungs from $p27^{kip1+/+}$, $p27^{kip1-/-}$ and $p27^{kip1}CK^{-}$ mice treated with urethane to induce lung tumour formation were described elsewhere (Serres et al., 2011). Paraffin sections were cleared and rehydrated tissue sections were steamed for 30 min in sodium citrate pH 6 unmasking solution and blocked in PBS 0.2% Triton-X100, 3% BSA and 10% donkey serum for 30 min at room temperature. For macrophage infiltration quantification assays, sections were stained using a rat anti-F4/80 antibody (AbD Serotec, Oxford, UK). Slides were then scanned using a Pannoramic 250 Flash II slide scanner (3DHISTECH, Budapest, Hungary) with a 20×magnification lens. Automatic quantification of macrophages on virtual slides was performed using a custom-made macro developed in ImageJ software. Briefly, colours were deconvoluted using a plugin by Gabriel Landini (http://www.mecourse.com/landinig/software/cdeconv/cdeconv.html) to separate staining of peroxydase substrate from hematoxylin coloration. A threshold on staining of peroxydase substrate was chosen manually to dissociate specific signal from the background. The average peroxidase-substrate-positive cell area was evaluated by dividing the peroxydase substrate area by the number of positive cells that were counted manually in an ~5000 µm^2 region. Tissues of interest were then delimited manually and the area of peroxidase-substrate-positive staining per tissue area was automatically measured. The density of peroxidase-substrate-positive cells was then deduced from the density of staining and the evaluation of average cell area. Statistical tests were performed on SigmaPlot 12.5 using One-Way ANOVA. For $p27^{kip1}$ cellular localisation assays, slides were stained simultaneously with rabbit anti-$p27^{kip1}$ (C-19, Santa-Cruz Biotechnology Inc., Dallas, TX), rat anti-F4/80 pan macrophage marker (BM8, AbD Serotec) and goat anti-surfactant protein-C (SP-C) (M-20, Santa-Cruz Biotechnology Inc.) antibodies as described previously (Besson et al., 2007; Serres et al., 2011). Samples were then incubated with the indicated primary antibodies for 1 h at 37℃. After rinsing, sections were incubated with secondary antibodies conjugated to either of the indicated fluorochromes (Cy2, Cy3 and Cy5) (Jackson ImmunoResearch Laboratories, Inc., Suffolk, UK) for 30 min. DNA was labelled with Hoechst 33304 added to the first wash after secondary antibody. After mounting of the slides, images were acquired on a Nikon Eclipse 90i microscope equipped with a CoolSnap HQ2 camera using the NIS-Br software (Nikon, Champigny-sur-Marne, France). The proportion of cells with cytoplasmic and/or nuclear localisation of $p27^{kip1}$ was

quantified on lung sections of three $p27^{kip1}CK^{-}$ and five $p27^{kip1+/+}$ mice using ImageJ. Statistics were performed using paired Student's *t*-test, two-tailed, 95% confidence interval.

Measurement of monocyte content in mice blood samples

Heparinised circulating blood was collected and the number of monocytes was measured by using the Micros 60 Hematology Analyzer (Horiba, Kyoto, Japan). Statistical analysis was performed with GraphPad Prism software.

Acknowledgements

We acknowledge Toulouse Réseau Imagerie for imaging, Brigitte Raynaud-Messina for critical reading of the manuscript and Annie Béhar for technical assistance.

Competing interests

The authors declare no competing interests.

Author contributions

P.G. and A.L. performed experiments, interpreted results and assisted with writing the manuscript; E.V.G. performed experiments on composite matrices; A.B. supplied mice and performed immunohistochemistry experiments; I.M.P. supervised the project and participated in writing the manuscript; V.L.C. performed experiments, interpreted results, directed the project and wrote the manuscript.

Funding

For this work, I.M.P. was supported by Fondation ARC pour la Recherche sur le Cancer [grant numbers 2010-120-1733 and ARC-Equipement 8505]; Agence Nationale de la Recherche (ANR) [grant number 2010-01301]; and Fédération pour la Recherche Médicale [grant number #FRM-DEQ 20110421312]; V.L.C. was supported by Région Midi-Pyrénées [grant number 10051286]; and Université de Toulouse III; A.B. was supported by Ligue Nationale contre le Cancer and Institut National du Cancer. P.G. was supported by a doctoral fellowship from Université de Toulouse III.

References

Baldassarre, G., Belletti, B., Nicoloso, M. S., Schiappacassi, M., Vecchione, A., Spessotto, P., Morrione, A., Canzonieri, V. and Colombatti, A. (2005). p27(Kip1)-stathmin interaction influences sarcoma cell migration and invasion. *Cancer Cell* **7**, 51-63.

Berton, S., Belletti, B., Wolf, K., Canzonieri, V., Lovat, F., Vecchione, A., Colombatti, A., Friedl, P. and Baldassarre, G. (2009). The tumor suppressor functions of p27(kip1) include control of the mesenchymal/amoeboid transition. *Mol. Cell. Biol.* **29**, 5031-5045.

Besson, A., Assoian, R. K. and Roberts, J. M. (2004a). Regulation of the cytoskeleton: an oncogenic function for CDK inhibitors? *Nat. Rev. Cancer* **4**, 948-955.

Besson, A., Gurian-West, M., Schmidt, A., Hall, A. and Roberts, J. M. (2004b). p27Kip1 modulates cell migration through the regulation of RhoA activation. *Genes Dev.* **18**, 862-876.

Besson, A., Gurian-West, M., Chen, X., Kelly-Spratt, K. S., Kemp, C. J. and Roberts, J. M. (2006). A pathway in quiescent cells that controls p27Kip1 stability, subcellular localization, and tumor suppression. *Genes Dev.* **20**, 47-64.

Besson, A., Hwang, H. C., Cicero, S., Donovan, S. L., Gurian-West, M., Johnson, D., Clurman, B. E., Dyer, M. A. and Roberts, J. M. (2007). Discovery of an oncogenic activity in p27Kip1 that causes stem cell expansion and a multiple tumor phenotype. *Genes Dev.* **21**, 1731-1746.

Biswas, S. K., Gangi, L., Paul, S., Schioppa, T., Saccani, A., Sironi, M., Bottazzi, B., Doni, A., Vincenzo, B., Pasqualini, F. et al. (2006). A distinct and unique transcriptional program expressed by tumor-associated macrophages (defective NF-kappaB and enhanced IRF-3/STAT1 activation). *Blood* **107**, 2112-2122.

Carragher, N. O. (2006). Calpain inhibition: a therapeutic strategy targeting multiple disease states. *Curr. Pharm. Des.* **12**, 615-638.

Carragher, N. O., Walker, S. M., Scott Carragher, L. A., Harris, F., Sawyer, T. K., Brunton, V. G., Ozanne, B. W. and Frame, M. C. (2006). Calpain 2 and Src dependence distinguishes mesenchymal and amoeboid modes of tumour cell invasion: a link to integrin function. *Oncogene* **25**, 5726-5740.

Cougoule, C., Le Cabec, V., Poincloux, R., Al Saati, T., Mège, J. L., Tabouret, G., Lowell, C. A., Laviolette-Malirat, N. and Maridonneau-Parini, I. (2010). Three-dimensional migration of macrophages requires Hck for podosome organization and extracellular matrix proteolysis. *Blood* **115**, 1444-1452.

Cougoule, C., Van Goethem, E., Le Cabec, V., Lafouresse, F., Dupré, L., Mehraj, V., Mège, J. L., Lastrucci, C. and Maridonneau-Parini, I. (2012). Blood leukocytes and macrophages of various phenotypes have distinct abilities to form podosomes and to migrate in 3D environments. *Eur. J. Cell Biol.* **91**, 938-949.

Denicourt, C., Saenz, C. C., Datnow, B., Cui, X. S. and Dowdy, S. F. (2007). Relocalized p27Kip1 tumor suppressor functions as a cytoplasmic metastatic oncogene in melanoma. *Cancer Res.* **67**, 9238-9243.

Doyle, A. D., Wang, F. W., Matsumoto, K. and Yamada, K. M. (2009). One-dimensional topography underlies three-dimensional fibrillar cell migration. *J. Cell Biol.* **184**, 481-490.

DuFort, C. C., Paszek, M. J. and Weaver, V. M. (2011). Balancing forces: architectural control of mechanotransduction. *Nat. Rev. Mol. Cell Biol.* **12**, 308-319.

Elkington, P. T. and Friedland, J. S. (2006). Matrix metalloproteinases in destructive pulmonary pathology. *Thorax* **61**, 259-266.

Even-Ram, S. and Yamada, K. M. (2005). Cell migration in 3D matrix. *Curr. Opin. Cell Biol.* **17**, 524-532.

Fero, M. L., Rivkin, M., Tasch, M., Porter, P., Carow, C. E., Firpo, E., Polyak, K., Tsai, L. H., Broudy, V., Perlmutter, R. M. et al. (1996). A syndrome of multiorgan hyperplasia with features of gigantism, tumorigenesis, and female sterility in p27(Kip1)-deficient mice. *Cell* **85**, 733-744.

Friedl, P. and Weigelin, B. (2008). Interstitial leukocyte migration and immune function. *Nat. Immunol.* **9**, 960-969.

Friedl, P. and Wolf, K. (2003). Proteolytic and non-proteolytic migration of tumour cells and leucocytes. *Biochem. Soc. Symp.* **70**, 277-285.

Fuster, J. J., González-Navarro, H., Vinué, A., Molina-Sànchez, P., Andrés-Manzano, M. J., Nakayama, K. I., Nakayama, K., Díez-Juan, A., Bernad, A., Rodríguez, C. et al. (2011). Deficient p27 phosphorylation at serine 10 increases macrophage foam cell formation and aggravates atherosclerosis through a proliferation-independent mechanism. *Arterioscler. Thromb. Vasc. Biol.* **31**, 2455-2463.

Guiet, R., Van Goethem, E., Cougoule, C., Balor, S., Valette, A., Al Saati, T., Lowell, C. A., Le Cabec, V. and Maridonneau-Parini, I. (2011). The process of macrophage migration promotes matrix metalloproteinase-independent invasion by tumor cells. *J. Immunol.* **187**, 3806-3814.

Guiet, R., Vérollet, C., Lamsoul, I., Cougoule, C., Poincloux, R., Labrousse, A., Calderwood, D. A., Glogauer, M., Lutz, P. G. and Maridonneau-Parini, I. (2012). Macrophage mesenchymal migration requires podosome stabilization by filamin A. *J. Biol. Chem.* **287**, 13051-13062.

Ishida, N., Kitagawa, M., Hatakeyama, S. and Nakayama, K. (2000). Phosphorylation at serine 10, a major phosphorylation site of p27(Kip1), increases its protein stability. *J. Biol. Chem.* **275**, 25146-25154.

Ishigami, S., Ueno, S., Nishizono, Y., Matsumoto, M., Kurahara, H., Arigami, T., Uchikado, Y., Setoyama, T., Arima, H., Yoshiaki, K. et al. (2011). Prognostic impact of CD168 expression in gastric cancer. *BMC Cancer* **11**, 106.

Jevnikar, Z., Mirković, B., Fonović, U. P., Zidar, N., Švajger, U. and Kos, J. (2012). Three-dimensional invasion of macrophages is mediated by cysteine cathepsins in protrusive podosomes. *Eur. J. Immunol.* **42**, 3429-3441.

Kalluri, R. (2003). Basement membranes: structure, assembly and role in tumour angiogenesis. *Nat. Rev. Cancer* **3**, 422-433.

Kawauchi, T., Chihama, K., Nabeshima, Y. and Hoshino, M. (2006). Cdk5 phosphorylates and stabilizes p27kip1 contributing to actin organization and cortical neuronal migration. *Nat. Cell Biol.* **8**, 17-26.

Kotake, Y., Nakayama, K., Ishida, N. and Nakayama, K. I. (2005). Role of serine 10 phosphorylation in p27 stabilization revealed by analysis of p27 knock-in mice harboring a serine 10 mutation. *J. Biol. Chem.* **280**, 1095-1102.

Luster, A. D., Alon, R. and von Andrian, U. H. (2005). Immune cell migration in inflammation: present and future therapeutic targets. *Nat. Immunol.* **6**, 1182-1190.

Mackay, C. R. (2008). Moving targets: cell migration inhibitors as new anti-inflammatory therapies. *Nat. Immunol.* **9**, 988-998.

Maruotti, N., Cantatore, F. P., Crivellato, E., Vacca, A. and Ribatti, D. (2007). Macrophages in rheumatoid arthritis. *Histol. Histopathol.* **22**, 581-586.

Nagahara, H., Vocero-Akbani, A. M., Snyder, E. L., Ho, A., Latham, D. G., Lissy, N. A., Becker-Hapak, M., Ezhevsky, S. A. and Dowdy, S. F. (1998). Transduction of full-length TAT fusion proteins into mammalian cells: TAT-p27Kip1 induces cell migration. *Nat. Med.* **4**, 1449-1452.

Pollard, J. W. (2009). Trophic macrophages in development and disease. *Nat. Rev. Immunol.* **9**, 259-270.

Porta, C., Riboldi, E., Totaro, M. G., Strauss, L., Sica, A. and Mantovani, A. (2011). Macrophages in cancer and infectious diseases: the 'good' and the 'bad'. *Immunotherapy* **3**, 1185-1202.

Qualls, J. E. and Murray, P. J. (2010). A double agent in cancer: stopping macrophages wounds tumors. *Nat. Med.* **16**, 863-864.

Rodier, G., Montagnoli, A., Di Marcotullio, L., Coulombe, P., Draetta, G. F., Pagano, M. and Meloche, S. (2001). p27 cytoplasmic localization is regulated by phosphorylation on Ser10 and is not a prerequisite for its proteolysis. *EMBO J.* **20**, 6672-6682.

Ruhrberg, C. and De Palma, M. (2010). A double agent in cancer: deciphering macrophage roles in human tumors. *Nat. Med.* **16**, 861-862.

Sahai, E. and Marshall, C. J. (2003). Differing modes of tumour cell invasion have distinct requirements for Rho/ROCK signalling and extracellular proteolysis. *Nat. Cell Biol.* **5**, 711-719.

Schindler, M., Nur-E-Kamal, A., Ahmed, I., Kamal, J., Liu, H. Y., Amor, N., Ponery, A. S., Crockett, D. P., Grafe, T. H., Chung, H. Y. et al. (2006). Living in three dimensions: 3D nanostructured environments for cell culture and regenerative medicine. *Cell Biochem. Biophys.* **45**, 215-227.

Serres, M. P., Zlotek-Zlotkiewicz, E., Concha, C., Gurian-West, M., Daburon, V., Roberts, J. M. and Besson, A. (2011). Cytoplasmic p27 is oncogenic and cooperates with Ras both in vivo and in vitro. *Oncogene* **30**, 2846-2858.

Shabo, I., Stål, O., Olsson, H., Doré, S. and Svanvik, J. (2008). Breast cancer expression of CD163, a macrophage scavenger receptor, is related to early distant recurrence and reduced patient survival. *Int. J. Cancer* **123**, 780-786.

Sherr, C. J. and Roberts, J. M. (1999). CDK inhibitors: positive and negative regulators of G1-phase progression. *Genes Dev.* **13**, 1501-1512.

Takai, Y., Sasaki, T. and Matozaki, T. (2001). Small GTP-binding proteins. *Physiol. Rev.* **81**, 153-208.

Tanaka, T., Nishimura, D., Wu, R. C., Amano, M., Iso, T., Kedes, L., Nishida, H., Kaibuchi, K. and Hamamori, Y. (2006). Nuclear Rho kinase, ROCK2, targets p300 acetyltransferase. *J. Biol. Chem.* **281**, 15320-15329.

Ueno, S., Sakoda, M., Kurahara, H., Iino, S., Minami, K., Ando, K., Mataki, Y., Maemura, K., Ishigami, S., Shinchi, H. et al. (2011). Safety and efficacy of early postoperative hyperbaric oxygen therapy with restriction of transfusions in patients with HCC who have undergone partial hepatectomy. *Langenbecks Arch. Surg.* **396**, 99-106.

Van Goethem, E., Poincloux, R., Gauffre, F., Maridonneau-Parini, I. and Le Cabec, V. (2010). Matrix architecture dictates three-dimensional migration modes of human macrophages: differential involvement of proteases and podosome-like structures. *J. Immunol.* **184**, 1049-1061.

Van Goethem, E., Guiet, R., Balor, S., Charrière, G. M., Poincloux, R., Labrousse, A., Maridonneau-Parini, I. and Le Cabec, V. (2011). Macrophage podosomes go 3D. *Eur. J. Cell Biol.* **90**, 224-236.

Vlach, J., Hennecke, S. and Amati, B. (1997). Phosphorylation-dependent degradation of the cyclin-dependent kinase inhibitor p27. *EMBO J.* **16**, 5334-5344.

Weber, C., Zernecke, A. and Libby, P. (2008). The multifaceted contributions of leukocyte subsets to atherosclerosis: lessons from mouse models. *Nat. Rev. Immunol.* **8**, 802-815.

Wiesner, C., El Azzouzi, K. and Linder, S. (2013). A specific subset of RabGTPases controls cell surface exposure of MT1-MMP, extracellular matrix degradation and three-dimensional invasion of macrophages. *J. Cell Sci.* **126**, 2820-2833.

Wiesner, C., Le-Cabec, V., El Azzouzi, K., Maridonneau-Parini, I. and Linder, S. (2014). Podosomes in space: Macrophage migration and matrix degradation in 2D and 3D settings. *Cell Adh. Migr.* **8**, 8.